Effect of the refractive index mismatch on light propagation through diffusive layered media

Fabrizio Martelli, Samuele Del Bianco, and Giovanni Zaccanti
Dipartimento di Fisica dell'Università degli Studi di Firenze and Istituto Nazionale per la Fisica della Materia, Via G. Sansone 1, 50019 Sesto Fiorentino, Firenze, Italy
(Received 4 February 2004; published 12 July 2004)

The effect of the refractive index mismatch on light propagation through diffusive layers has been investigated. The refractive index mismatch changes the balance of energy inside the medium determining a temporal and spatial redistribution of light. Light penetration through the medium is obstructed (facilitated) by a negative (positive) refractive index step variation. An analytical solution of the time-dependent diffusion equation that accounts for this effect has been obtained. The solution has been validated by comparisons with the results of Monte Carlo simulations. An excellent description of light propagation is given even for a high refractive index mismatch.

DOI: 10.1103/PhysRevE.70.011907 PACS number(s): 87.10.+e, 87.64.Cc, 42.25.Dd, 05.60.Cd

I. INTRODUCTION

The diffusion equation (DE) is widely used in many fields of applied physics. In the last decades the DE has been particularly used for modeling light propagation through biological tissues or in general through highly scattering media. Many applications based on the use of near-infrared light for tissue spectroscopy [1] or for biomedical imaging instruments [2,3] require an accurate modeling of photon migration through tissues. Usually a set of measurements is carried out at the surface of tissue and subsequently it is used to retrieve the internal optical properties of tissue. An essential point of any retrieval lies in the model used for light propagation that should be able to represent with fine details the structure of the investigated medium. Biological tissue is characterized by a complex architecture and a correct modeling of its internal structure may be difficult. In a physical sense biological tissue is not a homogeneous medium. The scattering process is determined by microscopic fluctuations of the refractive index n between cells membranes, organelles, etc. The refractive index of bulk tissues is the result of many microscopic processes. Different types of tissue show different values of n, for instance 1.39 (muscle) and 1.45 (normal adipose tissue) [4]. The refractive index mismatches on a macroscopic scale, e.g., between fat and muscle or between skin and skull, determine refraction of light. These differences of the refractive index of different tissue types are usually neglected and n is then considered for most tissues a constant value around 1.4. This approximation may affect the analysis of measurements from biological tissue. There are difficulties in making accurate measurements of the refractive index of different tissue type. For this reason is not easy to establish the actual effects of refractive index variations in tissue. Despite this, it is important to develop a good modeling of the phenomenon since this is the base of any understanding of it.

The use of the DE to analyze experimental data from tissue has been mostly based on the assumption of a constant refractive index inside tissue. Some theoretical approaches have been proposed to account for the effects of refractive index variations within the DE. Aronson [5] and Faris [6] described the boundary conditions at the diffuse-diffuse interface where variations of the refractive index could be accounted for. Walker *et al.* [7] obtained an analytical solution for retrieving the optical properties of an inhomogeneity embedded in a homogenous highly scattering medium. The refractive index of the object was considered as an independent unknown together with its absorption and reduced scattering coefficient. Ripoll and Nieto-Vesperinas [8] derived the integral equations for diffuse photon density waves where boundary conditions corresponding to a diffuse-diffuse interface with index mismatch were considered. Recently, Dehghani *et al.* [9] studied the effects of internal refractive index variation in near-infrared optical tomography by use of a finite element modeling approach for a two-layered medium.

In this paper we derive a time-domain analytical solution of the DE for a layered medium that takes into account step variations between the refractive indices of the diffusive layers and between the layers and the external. The theory, that is an extension of a previous work [10], models a step change of the refractive index that results in a discontinuity of the photon fluence rate at the interface between two layers. A validation of the analytical solution is provided making a comparison with the results of Monte Carlo (MC) simulations. The effect of the refractive index mismatch is summarized by some maps of the irradiance inside the medium. The use of the theory in inversion procedures is straightforward since it is basically similar to procedures previously developed [11].

The theory is described in Sec. II. In Sec. III comparisons between the analytical theory and MC results are presented. Conclusions are in Sec. IV.

II. THEORY

We analyze the case of a parabolic-type time-dependent DE [12] with discontinuous coefficients, i.e., absorption coefficient μ_a, diffusion coefficient D, and refractive index n, which can vary inside the medium. The DE is solved making use of the eigenfunctions method. We have extended the method proposed by Zauderer (see Ref. [13], pp. 335–338) and subsequently developed by Martelli *et al.* [10] for the photon migration through a layered medium. The analytical

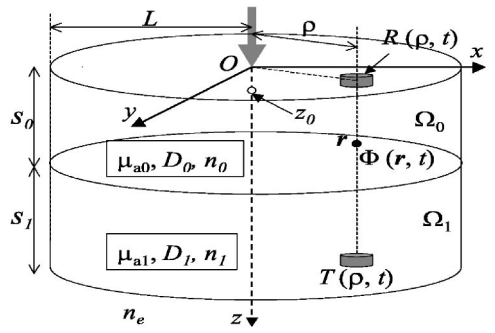

FIG. 1. Two-layered cylinder illuminated by a pencil light beam along the axis of the cylinder (z axis). L is the radius of the cylinder; s_0 and s_1 are the thickness of the top and bottom layers, respectively; μ_{a0}, μ_{a1} are the absorption coefficients, D_0, D_1 are the diffusion coefficients, and n_0, n_1 are the absolute refractive indices of the first and second layer, respectively. $R(\rho,t)$ and $T(\rho,t)$ are the reflectance and transmittance.

solution derived in Ref. [10] accounts for a different μ_a and a different reduced scattering coefficient μ_s' ($\mu_s'=1/3D$) [14]) of the diffusive layers, but n was assumed constant inside the medium. In Ref. [10] a layered parallelepiped was considered for the case of an isotropic Dirac-δ source term. Here, for simplicity, we refer to a two-layered cylinder as shown in Fig. 1. The theory, following the suggestions provided in this section, can be also extended to a three-layered cylinder.

Figure 1 shows the medium Ω composed of two regions: $\Omega=\Omega_0\cup\Omega_1$. In the figure s_0 and s_1 are the thickness, μ_{a0}, μ_{a1} the absorption coefficients, D_0, D_1 the diffusion coefficients, and n_0, n_1 the absolute refractive indices of the first and of second layer respectively. n_e is the absolute refractive index of the surrounding medium. The radius of the cylinder is assumed to be L. The origin of the reference system is chosen as the point where a collimated laser beam (propagating along the z axis) impinges normally the medium along the main axis of the cylinder; therefore its physical boundaries belong to the planes $z=0$ and $z=s_0+s_1$ and to the surface $\rho=L$. Let us consider a source term represented by a single isotropic point source placed in $\boldsymbol{r}_0=(0,0,z_0)$, i.e., $S(\boldsymbol{r},t)=\delta(\boldsymbol{r}-\boldsymbol{r}_0)\delta(t)$. The diffusion equation for the irradiance, Φ, is written as (v is the speed of light):

$$\left[\frac{1}{v}\frac{\partial}{\partial t}+\mu_a-\nabla[D(\boldsymbol{r})\nabla]\right]\Phi(\boldsymbol{r},t)=\delta(\boldsymbol{r}-\boldsymbol{r}_0)\delta(t). \qquad (1)$$

We follow a similar procedure to that described by Martelli *et al.* [10]. In deriving the solution we point out the differences, with this previous work, arised from the step variations of the refractive index. Because of the discontinuities of the optical properties across the plane $z=s_0$, we expect to find a solution of Eqs. (1) having some discontinuities. The problem must be separated in the two layers and can be stated as an initial-boundary value problem as the following:

$$\begin{cases}[\partial/(v_0\,\partial t)+\mu_{a0}-D_0\nabla^2]\Phi_0(\boldsymbol{r},t)=0, & t>0, \quad 0\leqslant z\leqslant s_0\\ [\partial/(v_1\,\partial t)+\mu_{a1}-D_1\nabla^2]\Phi_1(\boldsymbol{r},t)=0, & t>0, \quad s_0\leqslant z\leqslant s_0+s_1\end{cases} \qquad (2)$$

and the initial-boundary value conditions:

$$\Phi_0(\rho=L,z,t)=\Phi_0(\rho,z=-2A(n_{0e})D_0,t)=0, \qquad (3)$$

$$\Phi_1(\rho=L,z,t)=\Phi_1(\rho,z=s_0+s_1+2A(n_{1e})D_1,t)=0, \qquad (4)$$

$$\Phi_0(\boldsymbol{r},t=0)=v_0\delta(\boldsymbol{r}-\boldsymbol{r}_0). \qquad (5)$$

Equation (5) represents the initial distribution of sources in the medium assuming $\boldsymbol{r}_0$ in the first layer. Equations (3) and (4) represent the boundary conditions with the external medium and are based on two different assumptions: the extrapolated boundary condition (EBC) [15] has been used on the upper and lower surface ($z=0$ and $z=s_0+s_1$), while the zero boundary condition (ZBC) [15,16] has been used at the lateral boundary $\rho=L$. With the EBC the fluence rate is assumed equal to zero at an extrapolated boundary outside the turbid medium at a distance $z_e=2AD$. The coefficient $A(n_{me})$ also includes the effect of reflections due to the refractive index mismatch n_{me} between the medium m and the surrounding e [15]. The ZBC simply assumes the fluence rate equal to zero at the physical boundary of the medium. The ZBC is more approximated [15,17]; however, its use on the lateral boundary significantly simplifies the problem here addressed. With the EBC we would obtain different lateral extrapolated boundaries in the different layers. The boundary conditions at the lateral boundary do not affect the reflectance and the transmittance unless the source or the receiver is close to the boundary.

To account for the effect of a step change in the refractive index at the interface $z=s_0$ proper boundary conditions need to be introduced. When $n_0\neq n_1$ the continuity of the irradiance at $z=s_0$ does not hold. The correct boundary condition for the irradiance at $z=s_0$ results in [5,6,8]

$$\Phi_1(\rho,z=s_0,t)-(n_1/n_0)^2\Phi_0(\rho,z=s_0,t)=E(n_1/n_0)J_z, \qquad (6)$$

where the expression for E can be found in Refs. [5,6,8] and J_z represents the component of the photon flux normal to the interface. Ripoll and Nieto-Vesperinas [8] have shown that for a wide range of values, e.g., relative refractive index between the layers $\leqslant 1.28$, the right term of the above equation can be neglected. For simplicity, we consider, at the interface $z=s_0$, the boundary conditions described by the left

side of Eq. (6) and by the continuity of the photon flux. Therefore they are

$$\begin{cases} \Phi_0(\rho, z = s_0, t) = (n_0/n_1)^2 \Phi_1(\rho, z = s_0, t) \\ D_0 \, \partial \Phi_0(\rho, z = s_0, t)/\partial z = D_1 \, \partial \Phi_1(\rho, z = s_0, t)/\partial z. \end{cases} \tag{7}$$

We have assumed that the flux vector $\boldsymbol{J}(\boldsymbol{r},t)$ and the irradiance $\Phi(\boldsymbol{r},t)$ are related by the Fick's law: $\boldsymbol{J}(\boldsymbol{r},t) = -D(\boldsymbol{r})\boldsymbol{\nabla}\Phi(\boldsymbol{r},t)$ (Ref. [13], pp. 163–165). We will search for a solution of the stated problem of the kind

$$\Phi(\boldsymbol{r},t) = \begin{cases} \Phi_0(\boldsymbol{r},t) = \rho_0(\boldsymbol{r})\,\eta(t), & 0 \leqslant z \leqslant s_0 \\ \Phi_1(\boldsymbol{r},t) = \rho_1(\boldsymbol{r})\,\eta(t), & s_0 \leqslant z \leqslant s_0 + s_1. \end{cases} \tag{8}$$

It is in fact obvious that the temporal evolution of Φ_0 and Φ_1 must be coincident if we want that the condition (7) is valid. We will also require that the functions $\rho_0(\boldsymbol{r})$ and $\rho_1(\boldsymbol{r})$ satisfy the conditions (3) and (4). After substitution of the expression (8) in the system (2), we are led to the following eigenvalues problem:

$$\begin{cases} d\eta(t)/dt = -\lambda\,\eta(t) \\ -D_0\nabla^2\rho_0(\boldsymbol{r}) + \mu_{a0}\rho_0(\boldsymbol{r}) = (\lambda/v_0)\rho_0(\boldsymbol{r}) \\ -D_1\nabla^2\rho_1(\boldsymbol{r}) + \mu_{a1}\rho_1(\boldsymbol{r}) = (\lambda/v_1)\rho_1(\boldsymbol{r}). \end{cases} \tag{9}$$

The system (9) can also be rewritten as

$$\begin{cases} d\eta(t)/dt = -\lambda\,\eta(t) \\ \nabla^2\rho_0(\boldsymbol{r}) + K_0^2\rho_0(\boldsymbol{r}) = 0 \\ \nabla^2\rho_1(\boldsymbol{r}) + K_1^2\rho_1(\boldsymbol{r}) = 0, \end{cases} \tag{10}$$

where K_0^2 and K_1^2 are given by the expressions

$$K_0^2 = (\lambda/v_0 - \mu_{a0})/D_0, \quad K_1^2 = (\lambda/v_1 - \mu_{a1})/D_1. \tag{11}$$

We note that because the diffusion operator is, inside domains with constant refractive index, self-adjoint and positive (Ref. [13], pp. 171–178), the parameter λ is real and non-negative. On the contrary, no assumption can be made on the sign of K_0^2 and K_1^2, and in general the Helmholtz equations [18] in the system (10) admit solutions both for positive and negative values of these parameters.

In order to solve the Helmholtz equations in Eq. (10) we use the separation of the variables method. Let us suppose that a complete orthogonal set of eigenfunctions is given by the expression

$$\rho_{ln}(r) = \begin{cases} \rho_{0ln} = J_0(K_l\rho)a_{n0}\,\sin(K_{ln0}z + \gamma_{n0}) & 0 \leqslant z \leqslant s_0 \\ \rho_{1ln} = J_0(K_l\rho)a_{n1}\,\sin(K_{ln1}z + \gamma_{n1}) & s_0 \leqslant z \leqslant s_0 + s_1, \end{cases} \tag{12}$$

where J_0 is the zero order Bessel function of integer order and a_{n0}, a_{n1} are coefficients to be determined. From the separation of the variables method, according to conditions (3) and (4) it is clear that K_l are the roots of the equation

$$J_0(K_lL) = 0, \tag{13}$$

and that the conditions

$$K_0^2 = K_l^2 + K_{ln0}^2,$$

$$K_1^2 = K_l^2 + K_{ln1}^2 \tag{14}$$

must be satisfied. We note that Eq. (12) satisfies the boundary conditions (3) and (4) if γ_{ln0} and γ_{ln1} are chosen as

$$\gamma_{ln0} = 2K_{ln0}A_{0e}D_0,$$

$$\gamma_{ln1} = -K_{ln1}(s_0 + s_1 + 2A_{1e}D_1). \tag{15}$$

The boundary conditions (7) applied to ρ_{0ln} and ρ_{1ln} yield the linear system of equations for a_{n0} and a_{n1}:

$$\begin{cases} a_{n0}\sin[K_{ln0}(s_0 + 2A_{0e}D_0)] + a_{n1}\sin[K_{ln1}(s_1 + 2A_{1e}D_1)](n_0/n_1)^2 = 0 \\ a_{n0}D_0K_{ln0}\cos[K_{n0}(s_0 + 2A_{0e}D_0)] - a_{n1}D_1K_{ln1}\cos[K_{ln1}(s_1 + 2A_{1e}D_1)] = 0. \end{cases} \tag{16}$$

The system (16) admits nontrivial solutions (a_{n0}, $a_{n1} \neq 0$) if and only if the determinant vanishes. Therefore, we are led to the transcendental equation for the eigenvalues:

$$\frac{1}{D_0K_{ln0}}\tan[K_{ln0}(s_0 + 2A_{0e}D_0)] = -\frac{1}{D_1K_{ln1}}\tan[K_{ln1}(s_1 + 2A_{1e}D_1)](n_0/n_1)^2. \tag{17}$$

As shown in Ref. [10], there is the possibility that either K_{ln0}^2 or K_{ln1}^2 are negative. Details about the imaginary roots of Eq. (17) can be found in Appendix A. These roots are fundamental to obtaining the solution of the DE for the problem here analyzed.

Let us now consider the temporal evolution of the irradiance, which is obtained by solving the first equation in Eq. (10). The general solution of our initial-boundary value problem can be written as [13,18,19]

$$\Phi(\boldsymbol{r},t) = \sum_{l,n=1}^{\infty} \alpha_{ln}\rho_{ln}(\boldsymbol{r})\exp(-\lambda_{ln}t). \tag{18}$$

The initial condition (5) is used to determine α_{ln} together with a condition necessary to have a set of orthonormalized eigenfunctions. According to Ref. [13] (pp. 335–338), Ref. [19] (pp. 157 and 248–249), and to the proper definition of scalar product for the eigenvalue problem of Eq. (10) we have

$$\alpha_{ln} = \frac{\left\{ v_0 \int_{\Omega_0} f(\boldsymbol{r}) \rho^*_{0ln}(\boldsymbol{r}) d\boldsymbol{r} + v_1 \int_{\Omega_1} f(\boldsymbol{r}) \rho^*_{1ln}(\boldsymbol{r}) d\boldsymbol{r} \right\}}{\left\{ v_0 \int_{\Omega_0} \rho_{0ln}(\boldsymbol{r}) \rho^*_{0ln}(\boldsymbol{r}) d\boldsymbol{r} + v_1 \int_{\Omega_1} \rho_{1ln}(\boldsymbol{r}) \rho^*_{1ln}(\boldsymbol{r}) d\boldsymbol{r} \right\}}, \tag{19}$$

with

$$f(\boldsymbol{r}) = \Phi(\boldsymbol{r}, t=0) = v_0 \delta(\boldsymbol{r} - \boldsymbol{r}_0) = \sum_{l,n=1}^{\infty} \alpha_{ln} \rho_{ln}(\boldsymbol{r}), \tag{20}$$

where we have used the definition of the scalar product in the space of the continuous functions in the region Ω [$\rho^*_{ln}(\boldsymbol{r})$ is the complex conjugate of $\rho_{ln}(\boldsymbol{r})$]. The choice of the coefficients a_{n0} and a_{n1} together with the boundary conditions assure that $\rho_{ln}(\boldsymbol{r})$ multiplied with α_{ln} determines a set of real and orthonormal functions **(**the proof of the orthogonality of the eigenfunctions $\rho_{ln}(\boldsymbol{r})$ can be obtained by following a similar procedure to that shown in Appendix B of Ref. [10]**)**. This set of eigenfunctions can generate all the solutions of the initial boundary value problem considered in Eqs. (2) consistent with the boundary conditions of Eqs. (3)–(5). Substituting the expression (12) in (19) we have

$$\alpha_{ln} = v_0^2 \, a^*_{n0} \sin^*(K_{ln0} z_0 + \gamma_{ln0}) / N^2_{ln}, \tag{21}$$

with

$$N^2_{ln} = \left\{ v_0 \int_{\Omega_0} \rho_{0ln}(\boldsymbol{r}) \rho^*_{0ln}(\boldsymbol{r}) d\boldsymbol{r} + v_1 \int_{\Omega_1} \rho_{1ln}(\boldsymbol{r}) \rho^*_{1ln}(\boldsymbol{r}) d\boldsymbol{r} \right\}. \tag{22}$$

Finally we are able to write the solution of our initial-boundary value problem as

$$\Phi(\boldsymbol{r}, t) = \begin{cases} \displaystyle\sum_{l,n=1}^{\infty} v_0^2 \, J_0(K_l \rho) |a_{n0}|^2 \sin(K_{ln0} z + \gamma_{ln0}) \times \sin^*(K_{ln0} z_0 + \gamma_{ln0}) \exp[-(K_0^2 D_0 + \mu_{a0}) v_0 t] / N^2_{ln}, & 0 \leqslant z \leqslant s_0 \\ \displaystyle\sum_{l,n=1}^{\infty} v_0^2 J_0(K_l \rho) a^*_{n0} a_{n1} \sin(K_{ln1} z + \gamma_{ln1}) \times \sin^*(K_{ln0} z_0 + \gamma_{ln0}) \exp[-(K_1^2 D_1 + \mu_{a1}) v_1 t] / N^2_{ln}, & s_0 \leqslant z \leqslant s_0 + s_1. \end{cases} \tag{23}$$

The coefficients a_{n0} and a_{n1}, according to the system (16), are not uniquely determined; however, their ratio is determined by the boundary condition for the irradiance of Eq. (7). Assuming $a_{n0}=1$ we can rewrite Eq. (23) as

$$\Phi(\boldsymbol{r}, t) = \begin{cases} \displaystyle\sum_{l,n=1}^{\infty} v_0^2 J_0(K_l \rho) \sin(K_{ln0} z + \gamma_{ln0}) \times \sin^*(K_{ln0} z_0 + \gamma_{ln0}) \exp[-(K_0^2 D_0 + \mu_{a0}) v_0 t] / N^2_{ln}, & 0 \leqslant z \leqslant s_0 \\ \displaystyle\sum_{l,n=1}^{\infty} v_0^2 J_0(K_l \rho) b_{ln1} \sin(K_{ln1} z + \gamma_{ln1}) \times \sin^*(K_{ln0} z_0 + \gamma_{ln0}) \exp[-(K_1^2 D_1 + \mu_{a1}) v_1 t] / N^2_{ln}, & s_0 \leqslant z \leqslant s_0 + s_1, \end{cases} \tag{24}$$

where b_{ln1} is given by

$$b_{ln1} = a_{n1} = \frac{\sin(K_{ln0} s_0 + \gamma_{ln0})}{\sin(K_{ln1} s_0 + \gamma_{ln1})} (n_1/n_0)^2 = -\frac{\sin[K_{ln0}(s_0 + 2A_{0e} D_0)]}{\sin[K_{ln1}(s_1 + 2A_{1e} D_1)]} (n_1/n_0)^2. \tag{25}$$

The expression for the factor N^2_{ln} can be found in Appendix B. Equation (24) represents the Green's function for the cylinder of Fig. 1 when the source term is placed in the first layer along the axis of the cylinder. In case z_0 belongs to the second layer the expression for the Green's function changes and a new expression for α_{ln} is obtained according to Eqs. (19) and (20). The expression of $\Phi(\boldsymbol{r}, t)$ for $z_0 > s_0$ is reported in Appendix C. We point out that the position where the isotropic source term is placed does not affect the eigenvalues λ_{ln} but only the coefficients α_{ln} by Eq. (19). Therefore, K^2_{ln0} and K^2_{ln1} are obtained as solutions of the transcendental equation (17) in the same way of the case $z_0 < s_0$. Assuming as first layer that where the source is located, i.e., according to Fig. 1 the layer where the origin of the reference system is fixed, we have that in all generality Eq. (24) represents the Green's function of the medium when the source term is placed along the axis of the cylinder. Thinking in terms of reflectance or transmittance emerging from the medium (see Fig. 1) we have that changing the position of the Dirac-δ source from one layer to the other it is equivalent to exchanging the expressions for reflectance and trasmittance.

In case the source term does not belong to the axis of the cylinder, we lose rotation symmetry around z and the eigenfunctions of the system cannot be represented anymore by Eq. (12). Therefore, we need to introduce in the eigenfunctions a component for the rotation around z in order to represent all the points in the x-y plane. This changes a little the final expression for the irradiance, but the whole frame of the procedure remains unchanged. Moreover, we point out that, provided the distance of the source term from the z axis is much lower than L, Eq. (24) is in general a good approximation of the Green's function.

Finally, we notice that from the expression of the irradiance (24) we can calculate the reflectance $R(\rho,t)$ and the transmittance $T(\rho,t)$ by using the meaning of the flux vector:

$$R(\rho,t) = \boldsymbol{J}(\rho,z=0,t)\cdot(-\boldsymbol{k}),$$

$$T(\rho,t) = \boldsymbol{J}(\rho,z=s_0+s_1,t)\cdot(\boldsymbol{k}), \tag{26}$$

where R and T are evaluated in an arbitrary points on the surface $z=0$ and $z=s_0+s_1$ respectively, and the flux vector is given by the Fick's law; $\boldsymbol{k}$ is the unit vector along the z axis. From Eq. (24) we can derive the following expressions for the reflectance (27) and transmittance (28) respectively:

$$R(\rho,t) = \sum_{l,n=1}^{\infty} v_0^2 D_0 K_{ln0} J_0(K_l\rho)\cos(\gamma_{ln0}) \times \sin^*(K_{ln0}z_0 + \gamma_{ln0})\exp[-(K_0^2 D_0 + \mu_{a0})v_0 t]/N_{ln}^2, \tag{27}$$

$$T(\rho,t) = -\sum_{l,n=1}^{\infty} v_0^2 D_1 K_{ln1} J_0(K_l\rho) b_{ln1}\cos[K_{ln1}(s_0+s_1)+\gamma_{ln1}] \times \sin^*(K_{ln0}z_0+\gamma_{ln0})\exp[-(K_1^2 D_1+\mu_{a1})v_1 t]/N_{ln}^2. \tag{28}$$

The whole procedure we described provides the time domain Green's function for a two-layered cylinder with variations between the refractive index of the layers illuminated by an isotropic light source placed in z_0. When a pencil light beam (z axis in Fig. 1) is normally impinging the medium some approximations need to be introduced. The real source term is substituted either by a line of isotropic sources or by a single isotropic point source located at $\boldsymbol{r}_0=(0,0,z_0)$ as considered in our derivation. The coordinate z_0 is obtained by imposing that the line of isotropic point sources and the single point source have the same first moment [10]. In accordance with this assumption if the thickness of the first layer is sufficiently large we have $z_0=1/(\mu'_{s0}+\mu_{a0})$, where μ'_{s0} and μ_{a0} are the reduced scattering coefficient and the absorption coefficient of the first layer. Although the more general line source can also be treated as simple integral by Eq. (19), in this paper we restrict our investigation to the single point source.

III. RESULTS

In a previous paper [10] we have already shown that a solution of the DE for layered media based on the eigenfunctions method is able to describe step variations of the absorption and of the reduced scattering coefficient of the layers. In this section we present a set of comparisons between the results of MC simulations and Eqs. (27) and (28) with the aim to show that the theory presented in Sec. II also provides an accurate description of step variations between the refractive indices of the layers, n_0 and n_1.

Details about the MC code can be found in Refs. [10,17]. For MC simulations we mainly used a scattering function of Rayleigh scatters for which the asymmetry factor g results to be =0. This choice of g, although is not realistic for biological tissues (for which in the near infrared range is $g\simeq 0.9$), allows us to reduce significantly the computation time of MC simulations. However, as expected by the DE, whenever we fixed the values of μ'_s in the different layers no significant differences were observed between MC results obtained for different combinations of scattering functions, i.e., different values of g, and scattering coefficients. Thus the validation of the theory shown in this section is, within the diffusion range, general and it does not refer to restricted conditions of light propagation. The MC code simulated a pencil light beam normally impinging the medium. The program for the solution of the DE is organized according to the details given in the previous section. It is worthwhile to remind that once a set of eigenvalues is calculated by solving the transcendental equation (17), we have all the useful information for the calculation of the Green's functions of the system at different source-detector distances. The roots of Eq. (17) have been found with a combination of bisection and Newton-Raphson methods [20].

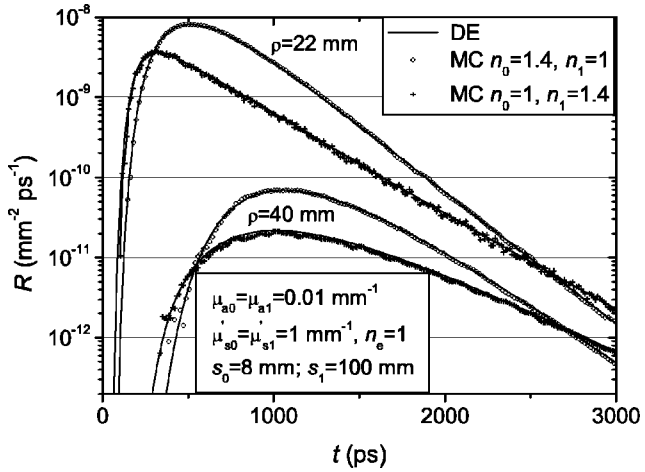

FIG. 2. Comparison between the time-resolved reflectance calculated with MC simulations (symbols) and with the DE (continuous curves) for a cylinder having: $s_0=8$ mm, $s_1=100$ mm, $L=100$ mm, $\mu_{a0}=\mu_{a1}=0.01$ mm^{-1}, $\mu'_{s0}=\mu'_{s1}=1$ mm^{-1}. Data are shown for $\rho=22$ and 40 mm for two values of the refrative index mismatch: $n_0=1.4$, $n_1=n_e=1$ (circles) and $n_0=n_e=1$, $n_1=1.4$ (crosses).

The results of Figs. 2–4 refer to a couple of diffusive layers that only differ by their refractive indices. In Fig. 2 some comparisons between MC (symbols) and DE (continuous lines) temporal profiles for the reflectance are shown. They refer to a cylinder having: $s_0=8$ mm, $s_1=100$ mm, $L=100$ mm, $\mu_{a0}=\mu_{a1}=0.01$ mm^{-1}, and $\mu'_{s0}=\mu'_{s1}=1$ mm^{-1}. The data are plotted for $\rho=22$ and 40 mm. Two values of the refractive index mismatch between the layers have been shown: $n_0=1.4$ and $n_1=n_e=1$, and $n_0=n_e=1$ and $n_1=1.4$.

In Fig. 3 some comparisons for the transmittance are shown. They refer to a cylinder having: $s_0=8$ mm, $s_1=12$ mm, $L=100$ mm, $\mu'_{s0}=\mu'_{s1}=1$ mm^{-1}. The curves are calculated at $\rho=0$ for $\mu_{a0}=\mu_{a1}=0.01$ mm^{-1} and for the nonabsorbing medium. Results are shown for $n_0=1.4$ and $n_1=n_e=1$, and $n_0=n_e=1$ and $n_1=1.4$. We notice that the results for the absorbing medium cannot be simply obtained by scaling the Green's function for the nonabsorbing medium with

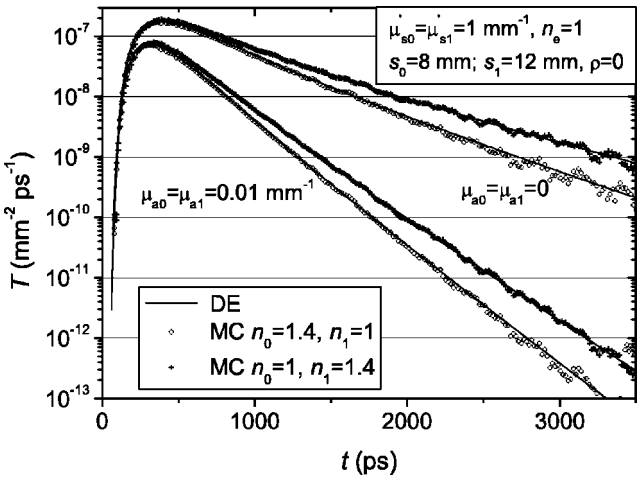

FIG. 3. Comparison between the time-resolved transmittance for a coaxial receiver ($\rho=0$) calculated with MC simulations (symbols) and with the DE (continuous curves). The cylinder has: $s_0=8$ mm, $s_1=12$ mm, $L=100$ mm, $\mu'_{s0}=\mu'_{s1}=1$ mm^{-1}. Data are shown for two values of the refractive index mismatch: $n_0=1.4$, $n_1=n_e=1$ (circles) and $n_0=n_e=1$, $n_1=1.4$ (crosses) both for $\mu_{a0}=\mu_{a1}=0.01$ mm^{-1} and for the nonabsorbing medium.

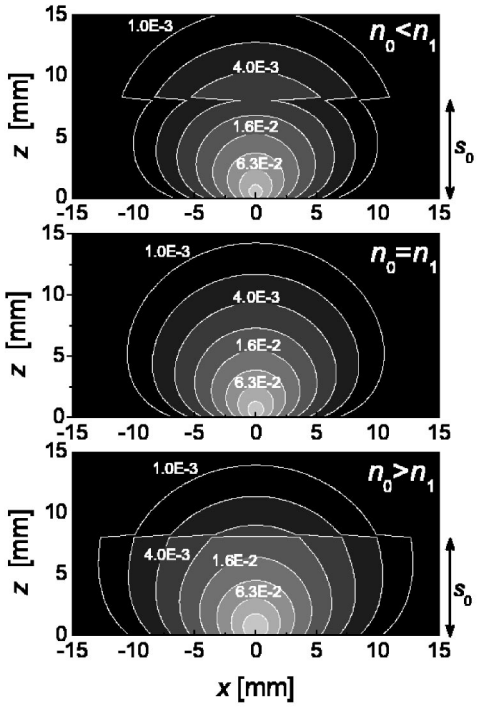

FIG. 4. Maps of the cw irradiance in the x-z plane for a layered cylinder having: $s_0=8$ mm, $s_1=100$ mm, $L=100$ mm, $\mu_{a0}=\mu_{a1}=0.01$ mm^{-1}, and $\mu'_{s0}=\mu'_{s1}=1$ mm^{-1}. The maps refer to: $n_0=n_e=1$, $n_1=1.4$ (top), $n_0=n_1=n_e=1$ (middle), and $n_0=1.4$, $n_1=n_e=1$ (bottom).

the exponential decay $\exp(-\mu_a vt)$ since we do not have an *a priori* knowledge of the time spent by received photons in the first and in the second layer.

Figure 4 shows maps of irradiance in the continuous wave (cw) domain. The cw irradiance has been obtained by an analytical integral of Eq. (24). The layered cylinder has: $s_0=8$ mm, $s_1=100$ mm, $L=100$ mm, $\mu_{a0}=\mu_{a1}=0.01$ mm^{-1}, and $\mu'_{s0}=\mu'_{s1}=1$ mm^{-1}. The maps refer to: $n_0=n_e=1$ and $n_1=1.4$ (top), $n_0=n_1=n_e=1$ (middle), and $n_0=1.4$ and $n_1=n_e=1$ (bottom). The refractive index mismatch determines a discontinuous behavior of the irradiance at the interface between the two layers, i.e., at $z=s_0=8$ mm. Photon migration through the second layer is obstructed (facilitated) when $n_0>n_1(n_0<n_1)$, i.e., a negative (positive) refractive index step variation between the layers determines a lower (higher) penetration depth of the diffuse light.

All the comparisons we presented show an excellent agreement between the results of the MC simulations and the theory derived in the preceding section. The formulas presented are able to account for significant variations between the refractive index of the diffusive layers. The computation time for any set of temporal profiles was always shorter than 1 s by using a 1.8-GHz Pentium IV processor.

IV. CONCLUSIONS

With the aim of modeling the refractive index mismatch inside layered media a Green's function of the time-domain diffusion equation for a layered cylinder where the source term is placed along the axis of the cylinder has been obtained by using the eigenfunctions method. The Green's function accounts for step variations of refractive index both between the diffusive layers and between the layers and the external. The refractive index mismatch at the interface of two diffusive layers results in a discontinuity of the photon fluence. To simplify the study of the problem we have used approximate boundary conditions expressed by Eq. (7). However, we have verified that this approximation does not significantly affect the results obtained. In fact, for all the cases analyzed in Figs. 2–4, we have repeated the calculations with the more correct boundary condition expressed by Eq. (6) (we notice that the use of this boundary condition makes the calculation quite more complicated) and we observed that the results did not change significantly even for a refractive index mismatch of 1.4. We therefore conclude that the range of refractive index mismatch for which the boundary condition expressed by Eq. (7) holds seems even larger than expected by the results of Ripoll and Nieto-Vesperinas [8].

The solution of the diffusion equation has been validated by comparisons with the results of Monte Carlo simulations. The correctness of the formulas presented in Sec. II has been verified for a wide range of the refractive indices n_0, n_1, and n_e. In conclusion, the proposed theory provides a fast, accurate, and reliable method to model the effect of the refractive index mismatch at the interface of two diffusive layers. The refractive index mismatch changes both the shape of the time-resolved reflectance or transmittance and the balance of energy inside the medium. In the analytical expressions of Sec. II the refractive index mismatch changes the distribution of eigenvalues, the normalization factor, and the speed of light passing through the layers.

Although the formulas presented in Sec. II may find applications in several physical processes, we make our final conclusion with some considerations on their use in tissue

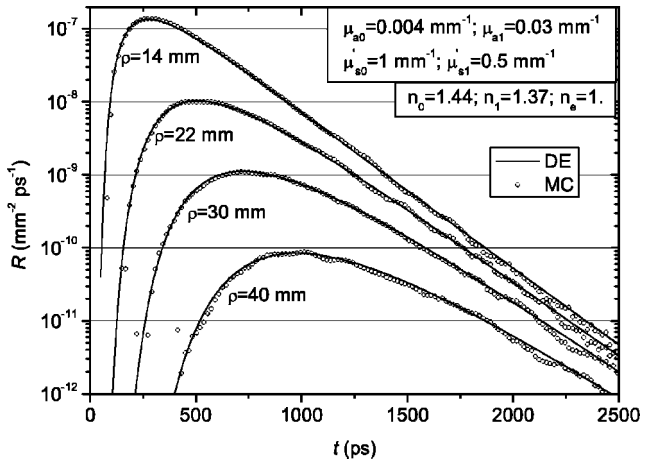

FIG. 5. Reflectance calculated with MC simulations (symbols) and with the solution of DE (continuous lines) for a cylinder having: $s_0=8$ mm, $s_1=100$ mm, $L=100$ mm, $\mu'_{s0}=1$ mm^{-1}, $\mu'_{s1}=0.5$ mm^{-1}, $\mu_{a0}=0.04$ mm^{-1} and $\mu_{a1}=0.03$ mm^{-1}, $n_0=1.44$, $n_1=1.37$, and $n_e=1$. The data are plotted for $\rho=14,22,30$, and 40 mm.

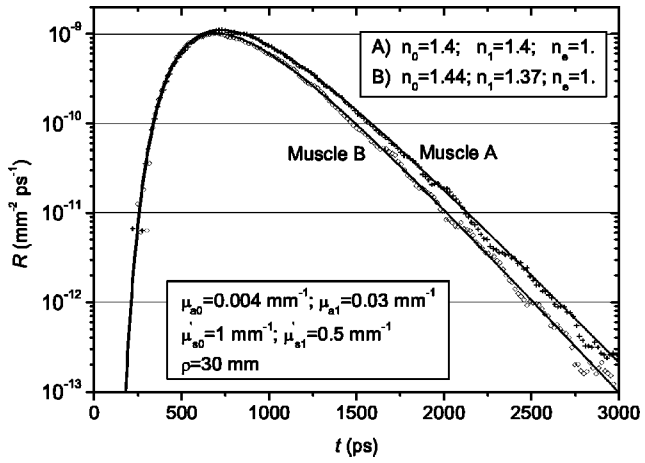

FIG. 6. Reflectance calculated with MC simulations (symbols) and with the solution of DE (continuous lines) for a cylinder having: $s_0=8$ mm, $s_1=100$ mm, $L=100$ mm, $\mu'_{s0}=1$ mm^{-1}, $\mu'_{s1}=0.5$ mm^{-1}, $\mu_{a0}=0.004$ mm^{-1}, and $\mu_{a1}=0.03$ mm^{-1}. The case Muscle A refers to $n_0=n_1=1.4$ and $n_e=1$, while the case Muscle B refers to $n_0=1.44$, $n_1=1.37$, and $n_e=1$. The data are plotted for $\rho=30$ mm.

spectroscopy. The internal optical properties of tissue are usually retrieved by inversion procedures on measurements carried out at the surface of the tissue. The theory and the results of Monte Carlo simulations have clearly shown that the refractive index mismatch may significantly change the time-resolved reflectance. Figures 5 and 6 refer to a couple of layers with optical properties similar to that of fat and of muscular tissue for which $\mu'_{s0}\neq\mu'_{s1}$, $\mu_{a0}\neq\mu_{a1}$, and $n_0\neq n_1$. In particular, Fig. 6 shows the effect that the refractive index variation determines on measurements of muscle oxygenation.

In Figs. 5 and 6 we have considered a two-layered cylinder with $s_0=8$ mm, $s_1=100$ mm, $L=100$ mm, $\mu_{a0}=0.004$ mm^{-1}, $\mu_{a1}=0.03$ mm^{-1}, $\mu'_{s0}=1$ mm^{-1}, and $\mu'_{s1}=0.5$ mm^{-1}. For modeling the optical properties of muscle with a subcutaneous fat layer we have chosen $n_0=1.44$ (representative of fat tissue, Ref. [21], p. 42) and $n_1=1.37$ (representative of muscular tissue, Ref. [21], p. 43). The good agreement in Fig. 5 between Eq. (27) and the results of MC simulations shows that the theory provides an accurate description of photon migration also when $\mu'_{s0}\neq\mu'_{s1}$, $\mu_{a0}\neq\mu_{a1}$, and $n_0\neq n_1$. In Fig. 6, for the distance $\rho=30$ mm we have compared the data of Fig. 5 with the data obtained assuming an average constant refractive index $n=n_0=n_1=1.4$. The differences between the curves denoted as Muscle A and Muscle B are representative of the error that may be encountered when a time-resolved measurement is analyzed with a model that does not account for refractive index variations. Therefore inversion procedures based on an average constant refractive index n lead to wrong estimation of the optical properties of the two layers. Equation (27) suggests that for the layer with refractive index larger than the average value n, μ_a would be underestimated and μ'_s overestimated and vice versa for the layer with lower refractive index. For the case of muscle with the fat layer errors remain within 5%.

The solution of the DE for the cylindrical geometry presented in this paper has the advantage, for the rotation symmetry around z, of a reduced computation time compared to that for the parallelepiped geometry [10]. The cylindrical geometry can be used to model measurements on biological tissues, for which the medium is usually assumed to be laterally infinite, provided a sufficient large radius of the cylinder is assumed [11].

ACKNOWLEDGMENT

The authors wish to thank Filippo Colomo for his help and for his useful suggestions.

APPENDIX A: IMAGINARY ROOTS

In Ref. [10] we analyzed the distribution of imaginary roots when the layers had matched refractive index but different absorption coefficient or different reduced scattering coefficient. In this appendix we summarize the changes that arise in the distribution of imaginary roots when a variation between the refractive indices of the diffusive layers is introduced. The initial-boundary value problem is thus solved after we determine the discrete number of solutions of the transcendental equation (17). As stated before, here we are looking at the possibility that either K^2_{ln0} or K^2_{ln1}, or both, are negative; therefore K_{ln0} and K_{ln1} are imaginary numbers. In fact it is possible to demonstrate that the transcendental equation (17) admits always imaginary roots whenever $(D_0/n_0)\neq(D_1/n_1)$. For the case $(D_0/n_0)=(D_1/n_1)$, imaginary roots are found only if a minimum criteria for the change of μ_a/n is met.

Let us start to write the relationship between K^2_{ln1} and K^2_{ln0} as

$$K^2_{ln1}=\frac{n_1}{n_0}\frac{D_0}{D_1}K^2_{ln0}+C, \tag{A1}$$

where

$$C = [(n_1/n_0)\mu_{a0} - \mu_{a1}]/D_1 + K_l^2[(n_1/n_0)D_0 - D_1]/D_1. \tag{A2}$$

We have a different linear relationship between K_{ln1}^2 and K_{ln0}^2 for $C>0$ and for $C<0$, respectively. For the case $K_{ln0}^2 < -(D_1/D_0)(n_0/n_1)C$ $(C>0)$, or $K_{ln0}^2<0 (C<0)$, possible roots K_{ln0} and K_{ln1} of Eq. (17) must be imaginary numbers: $K_{ln0} = \pm i|K_{ln0}|$, $K_{ln1} = \pm i|K_{ln1}|$. By using the property $\tanh(z) = -i \tan(iz)$, where z is a complex number, Eq. (17) becomes

$$\frac{\tanh[\pm|K_{ln0}|(s_0 + 2A_{0e}D_0)]}{D_0(\pm i|K_{ln0}|)} = -\frac{\tanh[\pm|K_{ln1}|(s_1 + 2A_{1e}D_1)]}{D_1(\pm i|K_{ln1}|)}(n_0/n_1)^2. \tag{A3}$$

We notice that Eq. (A3) is impossible; therefore our problem cannot admit eigenvalues with both K_{ln0}^2 and K_{ln1}^2 negative. In terms of the eigenfunctions it means that no eigenfunction has a component along the z axis given by a combination of exponential functions at both sides of the discontinuity $z=s_0$. Let us now treat separately the two possibilities $C>0$ and $C<0$ to search for imaginary roots of Eq. (17).

(i) $C>0$. Possible imaginary roots are found in the interval $-(D_1/D_0)(n_0/n_1)C<K_{ln0}^2<0$. Here we are looking at the possibility that Eq. (17) is solved for $K_{ln0}=\pm i|K_{n0}|$, and $K_{nl1}=\pm|K_{ln1}|$. The four different choices for the sign of K_{ln0} and K_{ln1} yield the same equation:

$$-\frac{\tanh[|K_{ln0}|(s_0 + 2A_{0e}D_0)]1}{D_0|K_{ln0}|} = \frac{\tan[|K_{ln1}|(s_1 + 2A_{1e}D_1)]}{D_1|K_{n1}|}(n_0/n_1)^2. \tag{A4}$$

Because we are studying Eq. (A4) in a limited interval of K_{ln0} and K_{ln1}, we notice that a necessary condition for Eq. (A4) to admit some roots is

$$\frac{\pi}{2} < \sqrt{C}\, l_1, \tag{A5}$$

where we have defined $l_1=s_1+2A_{1e}\, D_1$. A sufficient condition for Eq. (A4) to admit some roots is

$$\pi < \sqrt{C}\, l_1. \tag{A6}$$

If $D_0/n_0>D_1/n_1$ surely the condition (A6) will be met for infinite choices of the K_l, and for each one of them Eq. (A4) admits a finite number of roots. If we define $\alpha_1 = |K_{ln1}|l_1$, and $M_0=\mathrm{int}[\sqrt{C}l_1/\pi]$ ("int" indicates the integer part of the division) all the possible roots are found when $\alpha_1 \in \bigcup_{j=1}^{M_0}((2j-1)\pi/2, j\pi) \cup (M_0\pi, \sqrt{C}l_1)$, for the case $M_0>0$. While for the case $M_0=0$ the possible root is found when $\alpha_1 \in (\pi/2, \sqrt{C}l_1)$. It is also possible that there exist at maximum a finite number of choices of K_l for which the condition (A5) is not met and therefore there are no roots of Eq. (A4).

If $D_0/n_0=D_1/n_1=D/n$ (when $C>0$ it means that $\mu_{a0}/n_0>\mu_{a1}/n_1$, a necessary condition for Eq. (A4) to admit a finite number of roots is

$$\frac{\pi}{2} < \sqrt{\left(\frac{(n_1/n_0)\mu_{a0} - \mu_{a1}}{D}\right)}l_1. \tag{A7}$$

It means that the change of μ_a/n between the layers must satisfy the following minimum criteria (necessary condition):

$$\Delta(\mu_a/n) = \mu_{a0}/n_0 - \mu_{a1}/n_1 > \left(\frac{\pi}{2}\right)^2\frac{D/n}{l_1^2}. \tag{A8}$$

If $D_0/n_0<D_1/n_1$, the condition that we are considering, $C>0$, is verified only for a finite number of choices of the K_l. Again Eq. (A4) has roots, if the condition (A6) is satisfied.

(ii) $C<0$. Possible imaginary roots are found in the interval $0<K_{ln0}^2<-(D_1/D_0)(n_0/n_1)C$. In this case we are searching for roots of Eq. (17) of the kind $K_{ln0}=\pm|K_{ln0}|$, and $K_{ln1}=\pm i|K_{ln1}|$. After substitution in Eq. (17) we obtain

$$\frac{\tan[|K_{ln0}|(s_0 + 2A_{0e}D_0)]}{D_0|K_{ln0}|} = -\frac{\tanh[|K_{ln1}|(s_1 + 2A_{1e}D_1)]}{D_1|K_{ln1}|}(n_0/n_1)^2. \tag{A9}$$

Necessary and sufficient conditions for Eq. (A8) to admit some roots are

$$\frac{\pi}{2} < \sqrt{-\left(\frac{D_1}{D_0}\right)C}l_0, \tag{A10}$$

$$\pi < \sqrt{-\left(\frac{D_1}{D_0}\right)C}\;\; l_0, \tag{A11}$$

respectively, where we have defined $l_0=s_0+2A_{0e}\, D_0$.

If $D_0/n_0<D_1/n_1$, surely the condition (A11) will be met for infinite choices of the K_l, and for each one of them Eq. (A9) admits a finite number of roots. If we define $\alpha_0=|K_{ln0}|l_0$ and $M_0=\mathrm{int}[\sqrt{-(D_1/D_0)(n_0/n_1)C}\; l_0/\pi]$, all the possible roots are found when $\alpha_0 \in \bigcup_{j=1}^{M_0}((2j-1)\pi/2, j\pi) \cup (M_0\pi, \sqrt{-(D_1/D_0)(n_0/n_1)C}\; l_0)$ for the case $M_0>0$, while for the case $M_0=0$ the possible root is found when $\alpha_0 \in (\pi/2, \sqrt{-(D_1/D_0)(n_0/n_1)C}\; l_0)$. It is also possible that there exist at maximum a finite number of choices of K_l for which the condition (A10) is not met and therefore there are no roots of Eq. (A9).

If $D_0/n_0=D_1/n_1=D/n$ (it means that $\mu_{a0}/n_0<\mu_{a1}/n_1$) the condition (A10) yields a necessary condition for the change of μ_a/n of the two layers:

$$\Delta(\mu_a/n) = (\mu_{a1}/n_1 - \mu_{a0}/n_0) > \frac{D/n}{l_0^2}\left(\frac{\pi}{2}\right)^2. \tag{A12}$$

If $D_0/n_0>D_1/n_1$, the condition that we are considering, $C<0$, is verified only for a finite number of choices of K_l. Again Eq. (A9) has roots, if the condition (A11) is satisfied.

We can summarize this study by stating that whenever $D_0/n_0 \neq D_1/n_1$ the transcendental equation (17) always admits imaginary roots for either K_{ln0} or K_{ln1}. While if $D_0/n_0 = D_1/n_1$, imaginary roots of Eq. (17) are possible only if $\Delta(\mu_a/n) > [\Delta(\mu_a/n)]_{min}$, and we have determined necessary (and sufficient) conditions for both cases $C>0$ and $C<0$.

Now let us treat again simultaneously the two possibilities $C>0$ and $C<0$. If $K_{ln0}^2>0$ ($C>0$), or $K_{ln0}^2 > -(D_1/D_0)(n_0/n_1)C$ ($C<0$) we are searching for real roots of the transcendental Eq. (17). For this case we have to solve Eq. (17), and because we are studying it in an interval not bounded, we will always find infinite roots.

Why are the imaginary roots of Eq. (17) so important? If we plot K_{ln1}^2vs K_{ln0}^2 we understand that whenever imaginary roots exist, they might yield the lowest eigenvalues and in particular the minimum eigenvalue λ_{min}. This is definitely the case if, for example, $\Delta(\mu_a/n)=0$, $D_0/n_0 > D_1/n_1$, and

$$\pi < \sqrt{C_{\min}}\, l_1, \tag{A13}$$

where C_{min} is the value of C calculated for the lowest K_l. It is obvious that the minimum eigenvalue dominates in the series solution (24) (especially at late time). Therefore a large error in the shape of the temporal profile is expected if λ_{min} is not properly calculated.

APPENDIX B: NORMALIZATION FACTOR

The expression for the factor N_{ln} is obtaned by Eq. (22) and results in

$$N_{ln}^2 = \pi[LJ_1(K_l)]^2\left\{ v_0\left[\frac{l_0}{2} - \frac{\sin(2K_{ln0}l_0)}{4K_{ln0}}\right] + \frac{v_1 n_1^4 \sin^2(K_{ln0}l_0)}{n_0^4 \sin^2(K_{ln1}l_1)}\left[\frac{l_1}{2} - \frac{\sin(2K_{ln1}l_1)}{4K_{ln1}}\right]\right\}, \tag{B1}$$

$$N_{ln}^2 = \pi[LJ_1(K_l)]^2\left\{ v_0\left[-\frac{l_0}{2} + \frac{\sinh(2|K_{ln0}|l_0)}{4|K_{ln0}|}\right] + \frac{v_1 n_1^4 \sinh^2(|K_{ln0}|l_0)}{n_0^4 \sin^2(K_{ln1}l_1)}\left[\frac{l_1}{2} - \frac{\sin(2K_{ln1}l_1)}{4K_{ln1}}\right]\right\}, \tag{B2}$$

$$N_{ln}^2 = \pi[LJ_1(K_l)]^2\left\{ v_0\left[\frac{l_0}{2} - \frac{\sin(2K_{ln0}l_0)}{4K_{ln0}}\right] - \frac{v_1 n_1^4 \sin^2(K_{ln0}l_0)}{n_0^4 \sinh^2(|K_{ln1}|l_1)}\left[\frac{l_1}{2} - \frac{\sinh(2|K_{ln1}|l_1)}{4|K_{ln1}|}\right]\right\}, \tag{B3}$$

which are valid for the cases when both K_{ln0} and K_{ln1} are real, when $K_{ln0}=i|K_{ln0}|$ and $K_{ln1}=|K_{ln1}|$, and $K_{ln0}=|K_{ln0}|$ and $K_{ln1}=i|K_{ln1}|$, respectively.

APPENDIX C: SOLUTION WITH $z_0 > s_0$

The Green's function for a two-layered cylinder when the source term is placed in the second layer, i.e., $z_0 > s_0$, is

$$\Phi(\boldsymbol{r},t) = \begin{cases} \displaystyle\sum_{l,n=1}^{\infty} v_1^2 J_0(K_l\rho)\sin(K_{ln0}z + \gamma_{ln0}) \times b_{ln1}^{*} \sin^{*}(K_{ln1}z_0 + \gamma_{ln1})\exp[-(K_0^2 D_0 + \mu_{a0})v_0 t]/N_{ln}^2, & 0 \leqslant z \leqslant s_0 \\ \displaystyle\sum_{l,n=1}^{\infty} v_1^2 J_0(K_l\rho) b_{ln1}\sin(K_{ln1}z + \gamma_{ln1}) \times b_{ln1}^{*} \sin^{*}(K_{ln1}z_0 + \gamma_{ln1})\exp[-(K_1^2 D_1 + \mu_{a1})v_1 t]/N_{ln}^2, & s_0 \leqslant z \leqslant s_0 + s_1. \end{cases} \tag{C1}$$

[1] R. Cubeddu, A. Pifferi, P. Taroni, A. Torricelli, and G. Valentini, Appl. Phys. Lett. **74**, 874 (1999).
[2] J. C. Hebden, A. Gibson, R. M. Yusof, N. Everdell, E. M. C. Hillman, D. T. Delpy, S. R. Arridge, T. Austin, J. H. Meek, and J. S. Wyatt, Phys. Med. Biol. **47**, 4155 (2002).
[3] A. Pifferi, P. Taroni, A. Torricelli, F. Messina, R. Cubeddu, and G. Danesini, Opt. Lett. **28**, 1138 (2003).
[4] F. P. Bolin, L. E. Preuss, R. C. Taylor, and R. J. Ference, Appl. Opt. **28**, 2297 (1989).
[5] R. Aronson, J. Opt. Soc. Am. A **12**, 2532 (1995).
[6] G. Faris, J. Opt. Soc. Am. A **19**, 519 (2002).
[7] S. A. Walker, D. A. Boas, and E. Gratton, Appl. Opt. **37**, 1935 (1998).
[8] J. Ripoll and M. Nieto-Vesperinas, J. Opt. Soc. Am. A **16**, 1947 (1999).
[9] H. Dehghani, B. Brooksby, K. Vishwanath, B. W. Pogue, and K. D. Paulsen, Phys. Med. Biol. **48**, 2713 (2003).
[10] F. Martelli, A. Sassaroli, S. Del Bianco, Y. Yamada, and G. Zaccanti, Phys. Rev. E **67**, 056623 (2003).
[11] F. Martelli, S. Del Bianco, and G. Zaccanti, Opt. Lett. **28**, 1236 (2003).
[12] J. J. Duderstadt and W. R. Martin, *Transport Theory* (Wiley-Interscience, New York, 1979).
[13] E. Zauderer, *Partial Differential Equations of Applied Mathematics*, 2nd ed. (Wiley-Interscience, New York, 1989).
[14] K. Furutsu and Y. Yamada, Phys. Rev. E **50**, 3634 (1994).
[15] D. Contini, F. Martelli, and G. Zaccanti, Appl. Opt. **36**, 4587 (1997).
[16] M. S. Patterson, B. Chance, and B. C. Wilson, Appl. Opt. **28**, 2331 (1989).

[17] F. Martelli, D. Contini, A. Taddeucci, and G. Zaccanti, Appl. Opt. **36**, 4600 (1997).
[18] G. B. Arfken and H. J. Weber, *Mathematical Methods for Physicists*, 4th ed. (Academic Press, New York, 1995).
[19] G. F. Roach, *Green Functions: Introductory Theory with Applications* (Van Nostrand Reinhold, London, 1970).
[20] W. H. Press, B. P. Flannery, S. A. Teukolsky, and W. T. Vetterling, *Numerical Recipes: The Art of Scientific Computing* (Cambridge University Press, Cambridge, U.K., 1988).
[21] V. Tuchin, *Tissue Optics: Light Scattering Methods and Instruments for Medical Diagnosis* (SPIE PRESS, Bellingham, WA, 2000).